Microstructural study of β treated grade 702 zirconium. Scanning electron microscopy and transmission electron microscopy, complementarity of two observational scales

Jérôme Crépin, Thierry Bretheau, Daniel Caldemaison, Alain Barbu, Gérard Jazkierowitcz

Microstructural study of β treated grade 702 zirconium. Scanning electron microscopy and transmission electron microscopy, complementarity of two observational scales

J. CREPIN, T. BRETHEAU, D. CALDEMAISON
Laboratoire de Mécanique des Solides, C.N.R.S. U.R.A. 317, Ecole Polytechnique, 91128 Palaiseau Cedex, France

A. BARBU, G. JAZKIEROWITCZ
Section d'Etude des Solides Irradiés, CEA /DTA /CEREM /SESI, Ecole Polytechnique, 91128 Palaiseau Cedex, France

In this study we focus on the precipitation of betagenic elements (Fe, Cr, Ni) that occurs during the bPa allotropic transition in zirconium. In particular its structural characteristics, morphology and their consequences for the mechanical behaviour of the material are probed. The observations are made by means of a scanning electron microscope and a transmission electron microscope. The results reveal the occurrence of a quasi-continuous single crystalline phase, produced by the precipitation of the betagenic additional elements which constitute the so-called lath boundaries. This phase forms a layer surrounding the laths in the bulk of the material. Its morphology could be assimilated to a net, created by precipitates with a size of several micrometres and linked by narrow bridges with a size of several hundred nanometres. The chemical composition of the precipitates are of the $Zr_x(Cr, Fe2)_{1-x}$ type with $x \leq 40\%$.

1. Introduction

Zirconium, a material mainly used in the nuclear industry, is characterized by the existence of two allotropic varieties, the β phase and the α phase which have body centred cubic (b.c.c) and hexagonally close packed (h.c.p) crystal structures respectively. The former is found above 1148 K and the latter below the same threshold.

Manufactured structures made from zirconium require hollow-ware and welding operations. During welding, the filler metal (liquid at first) and the surrounding material which sustains an increase in temperature, go through the $\beta \rightarrow \alpha$ allotropic transition. Consequently a microstructural gradient and some precipitation occur; these heterogeneities are thought to influence the mechanical characteristics of the structure [1].

The aim of this study is focused on the study of the precipitation of betagenic elements (Fe, Cr, Ni) that occurs during the $\beta \rightarrow \alpha$ allotropic transition. In particular the structural characteristics, morphology and consequences for the mechanical behaviour are investigated. The observations are made by means of scanning electron microscopy (SEM) and transmission electron microscopy (TEM); indeed only a study at these two observational scales allows us to fully characterize the location, morphology, distribution, chemical composition and crystallographic orientation of the precipitates in the zirconium matrix.

Several authors [2–7] have reported that the size of the precipitates observed in zirconium and zirconium alloys is on the scale of hundreds of nanometres (Fig. 1) [4], whereas SEM observations suggest a size of several micrometres (Fig. 2a and b). Such a discrepancy requires an explanation especially because of the different roles, such differently sized precipitates can play with respect to plastic deformation and damage nucleation.

2. Material composition and allotropic transformation mechanisms

The $\beta \rightarrow \alpha$ transformation is martensitic or bainitic which always involve a shear process. The crystallographic relations arising from shear transformation between the b.c.c and h.c.p zirconium were first proposed by Burgers [8]. Each β grain can be transformed into at most 12 α variants, i.e., 6 (1 1 0) planes $\times$ 2$\langle$1 1 1$\rangle$ shear directions. The value of the angle between the basal planes of each h.c.p crystal pair can be either 0, 60 or 90° [9]. The nucleation rate, and therefore the number of activated variants, is a function of the cooling rate θ. As a consequence, the final microstructures can vary from a martensitic

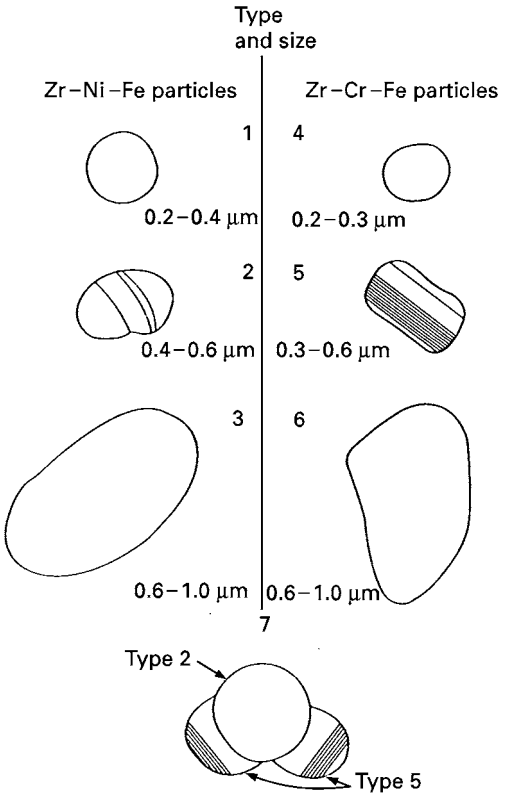

Figure 1 The shape, size and some substructure characteristics of Zr–Ni–Fe and Zr–Cr–Fe intermetallic particles are schematically shown. Types 1–3 contain Zr, Ni and Fe, while Types 4–6 are composed of Zr, Cr, and Fe. The type 7 morphology is a cluster consisting of a central Type 2 particle flanked by Type 5 particles. P. Chemelle *et al.* [4].

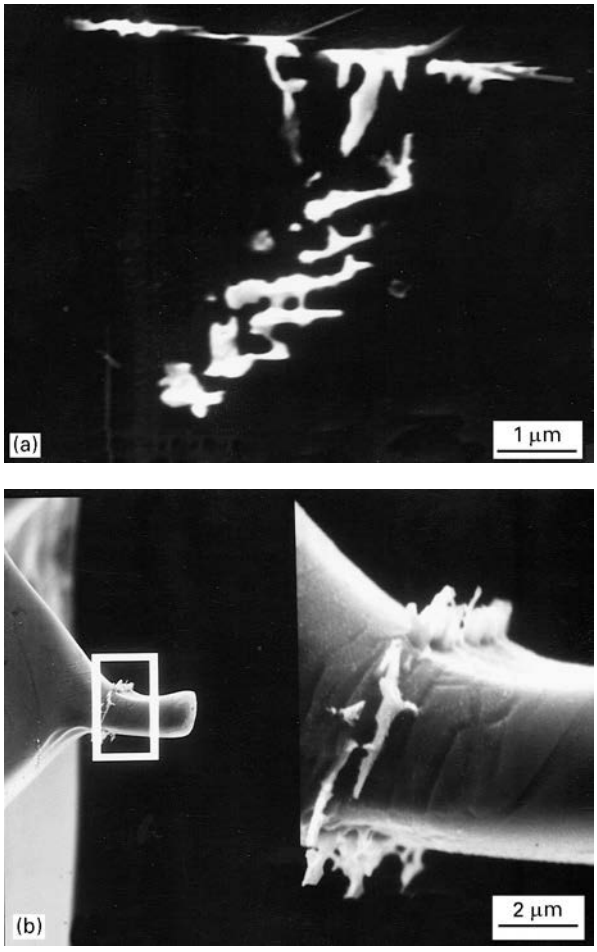

Figure 2 Precipitates observed in zirconium grade 702 β treated, after electrolytical polishing and chemical etching. (a) Surface of the sample after 5 seconds etching. (b) Edge of the sample after important dissolution.

microstructure to a Widmanstätten microstructure [10, 11]. For slow cooling rates ($\theta = 15\,^{\circ}s^{-1}$) the microstructure is characterized by the occurrence of colonies composed of parallel laths with the same crystallographic orientation. The interfaces or boundaries between these laths are the sole areas of precipitation of the additional elements. Each lath originates from a nucleus which appears at the boundary of the β grains. The lath's growth extends from the boundary towards the β grain centre. During the $\beta \rightarrow \alpha$ transformation the betagenic elements diffuse from the α nuclei to the β phase which has not yet transformed. The type of activated nucleus depends only on the characteristics of the boundary between two neighbouring β grains. Therefore only one type of colony exists at each boundary (Fig. 3) [12].

A rolled plate of grade 702 zirconium is used as the base material. 99.5 wt% is zirconium and the composition of the last 0.5 wt% is listed in Table I. Two types of elements have to be specified: the alphagenic elements (O, Sn) are in solid solution at room temperature, and the betagenic elements (Fe, Cr, Ni) in solid solution in the β phase, form precipitates in the α phase.

This plate has undergone an $\alpha \rightarrow \beta \rightarrow \alpha$ cycle, (maintained at 1523 K for 1 h in the β phase and cooled at a rate $\theta \approx 15\,^{\circ}s^{-1}$), similar to the one produced during a welding operation, to investigate the resulting microstructure.

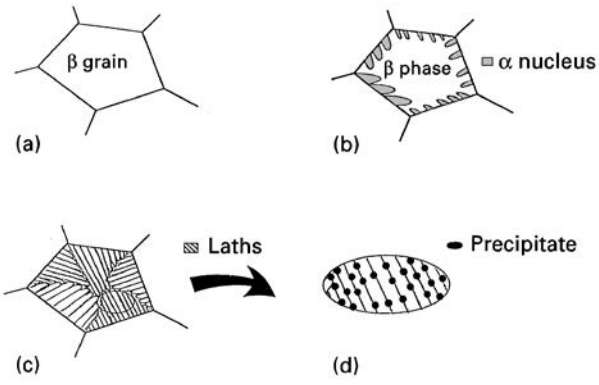

Figure 3 A simplified diagram of the $\beta \rightarrow \alpha$ microstructure transformation. (a) Microstructure before transformation (β phase). (b) $\beta \rightarrow \alpha$ transformation. (c) Microstructure after transformation (α phase). (d) Localization of the precipitates on the lath boundaries.

3. Observations at the scanning electron microscope scale

The microstructure (Fig. 4) is observed after a mechanical and electrolytical polishing (tension, U = 22 V, temperature, T = 300 K, time, t = 30 s, in CH_3COOH: 80%, $HClO_4$: 20%). The electron backscattering diffraction (EBSD) technique allows us to verify that the Burgers relations [9] between colonies stemmed from the same former β grain are respected; the angle of misorientation between the *c* axis of two

TABLE I Chemical composition (wt %) of the trace impurities in grade 702 zirconium

Elements	C	H	O	N	Cr	Fe	Ni	Sn
Analysis (10^{-3})	5.8	0.4–0.7	140	3.3	24	76	5	228

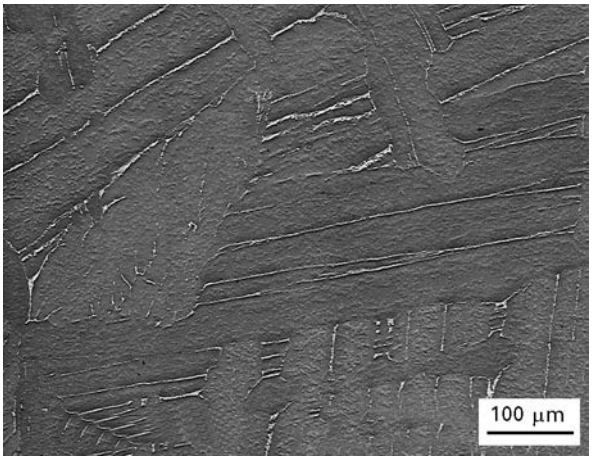

Figure 4 Observation of the microstructure after an electrolytical polishing and a slight chemical etching.

different colonies is either 60 or 90° (Fig 5a and b). In a previous study [12] we have shown that the alphagenic elements (O, Sn) are in solid solution; they are heterogeneously distributed with a high concentration in the centre of the lath and at a lower concentration in the vicinity of the lath boundaries (Fig. 6). Oxygen and tin are principally added in order to increase the critical resolved shear stress (CRSS) of all the deformation mechanisms, either crystallographic slip or twinning [13–16], which improves the mechanical characteristics of the material. The main consequence of the heterogeneity is the occurrence of a concentrated glide in narrow bands near the lath boundaries for the favourably oriented colonies [12].

Chemical etching (HF: 22%, HNO_3: 11%, glycerol: 67%, $T = 300\,K$, $t \cong 5\,s$) reveals the location of the betagenic elements (Fe, Cr, Ni). They form precipitates that are localized in the lath boundaries (Fig. 2a). The size of these precipitates is of the order of several micrometres (Fig. 2b). Successive dissolutions show that these precipitates form a layer around the laths in the bulk of the material. A qualitative analysis performed by energy dispersive spectroscopy (EDS) shows that the precipitates contain significant amounts of Zr, Fe and Cr, with a lower content of Ni. Precipitates containing these elements have often been reported [2–7] in the literature at two main compositions $Zr_2(Fe, Ni)$ and $Zr(Fe, Cr)_2$. However different compositions can also be observed depending on the thermal cycle undergone by the material. In any case the reported size of the precipitates is of the order of a 100 nm. One might wonder if the discrepancy in the sizes measured by SEM and by TEM could be an artifact due to the observation method.

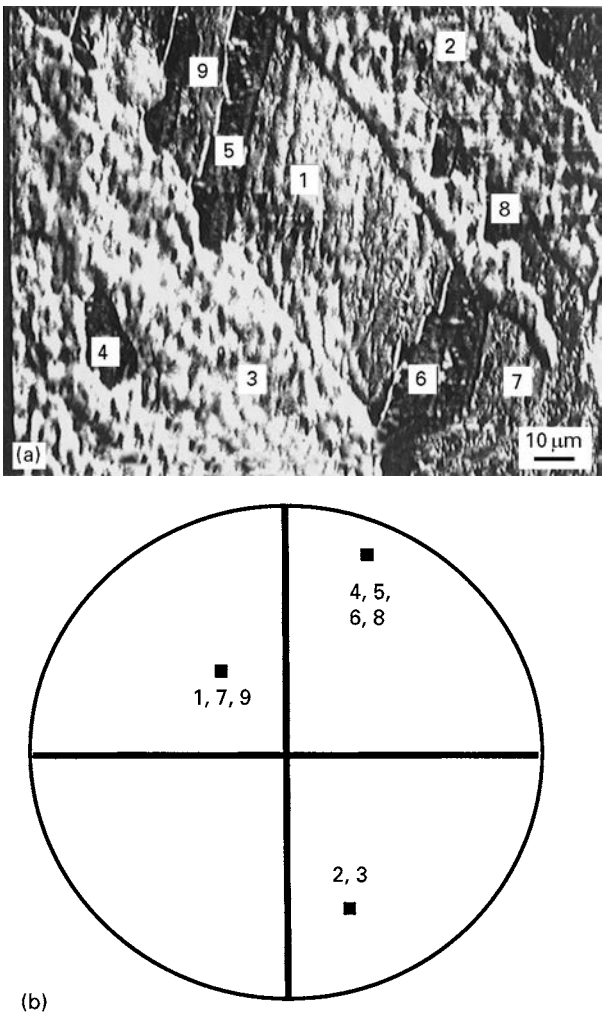

Figure 5 EBSP analysis of the orientation of three colonies stemmed from the same former β grain. (a) Observation of the surface sample tilted at 60°. (b) (0002) pole figure resulting from the EBSP analysis.

4. Observations at the transmission electron microscope scale

4.1. Size of precipitates

The size of the precipitates, located on the lath boundary that can be observed in Fig. 7 is between 100–350 nm; which is in agreement with the observations made previously by other authors. However these observations can only be performed near the hole in the thin foil, where the thickness is about 100 nm. Of course if the characteristic size of the microstructure is larger than the thickness of the thin foil then the image gives only a cross-section of it from which it is difficult or even impossible to deduce the true dimensions. However it is always possible to produce an X-ray image inside thicker areas of the thin foil using EDS techniques. In the case of β treated grade 702 zirconium, precipitates can be easily found because they are localized on the lath boundaries that are relatively straight. In this case the alignment of small precipitates observed in a thin area (Fig. 7) give the direction for the observation of thicker areas that would be more representative of the bulk of the material. The resulting X-ray image observations are presented in Fig. 8 which shows the iron distribution. It appears that the individual precipitates observed near

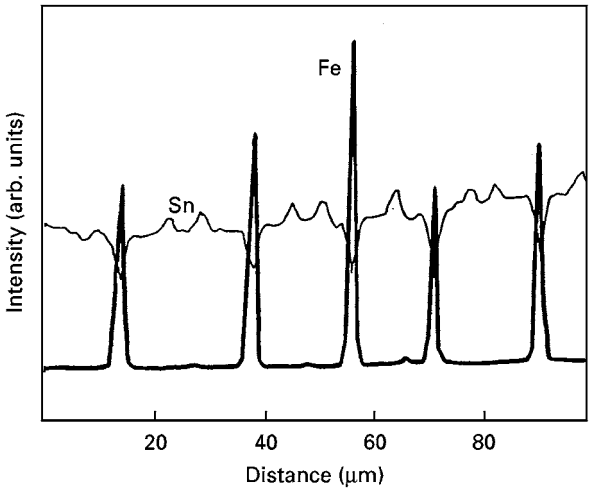

Figure 6 Tin and iron profiles across six laths. Iron is localized in the lath boundaries, and missing in the centers of the laths. On the other hand, tin is missing in the lath boundaries and is present in the center of the laths. Experimental conditions: 20 KeV; 0.5 μm pitch; 30 seconds per data.

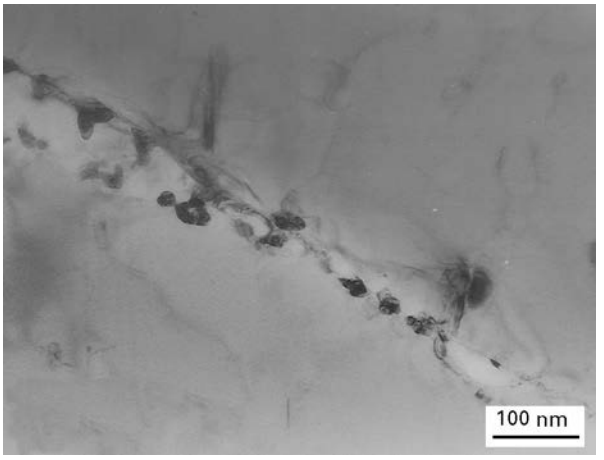

Figure 7 Observation of an alignment of precipitates in a thin foil from the hole to the bulk of the material.

the hole where the foil is thin (area A) become continuous at larger thickness (area B); in this area the width of this alignment is cons(tant and is about 0.5 μm. These observations complement those made using the SEM and allow us to conclude that the lath boundaries are decorated by precipitates with a size of the order of a few micrometres and linked to one another by "bridges". These bridges have a dimension close to 700 nm. The images allow us to assume that the alignment of precipitates forms a quasi-continuous phase. Then the discrepancy in the precipitate size observed by SEM and TEM is only a consequence of the difference in size of the observable volume.

4.2. Crystallographic relation between precipitates aligned along a lath boundary

The study of the crystallographic orientation of some precipitates located in the same alignment is performed on an area of Fig. 7. The micromicro diffraction carried out with a spot size of 30 nm is used. The

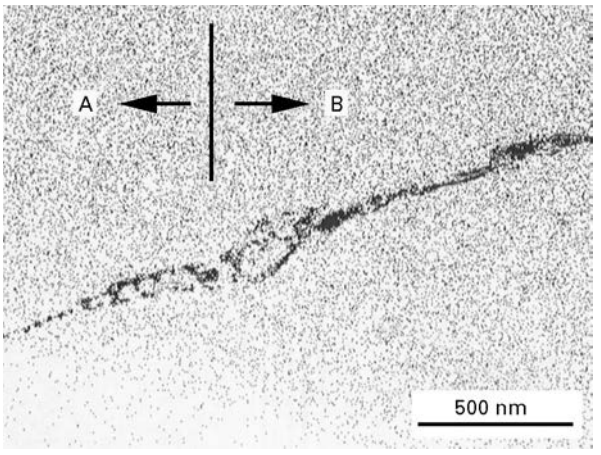

Figure 8 X-ray cartography of Fe performed on the precedent thin foil. Zone A corresponds to the area of Fig. 7 near the hole; zone B corresponds to the area in the bulk of the material. The alignment becomes continuous and larger from the zone A to the zone B.

locations of the analysed zones and the corresponding diffraction pattern area are presented in Fig. 9. If the orientation of two adjacent laths are different, they do not belong to the same colony. However the crystallographic orientation of the analysed precipitates are identical. This result allows us to conclude that the precipitates form more than a quasi-continuous phase, and in fact form a single crystalline phase along each lath boundary. This study will be extended to the investigation of potential epitaxial relationships between the precipitates and matrix.

4.3. Chemical composition

The chemical composition of the precipitates at a local level is obtained using EDS techniques using a beam diameter of 20 nm. The results are presented in Table II. The concentration ratio of Cr/Fe is approximately constant and equal to 0.5; the apparent variation of Zr concentration is probably due to the Zr rich matrix contribution. Consequently the precipitates are of the $Zr_x(Cr, Fe_2)_{1-x}$ type with $x \leqslant 40\%$. These results are in good agreement with those of Van der Sand and Bement [2]. This is principally due to the fact that the proportion of Fe and Cr in the chemical composition of the materials is of the same order in both cases (0.475 for the material investigated by Van der Sand and Bement: 0.35 in our case). In the other reports in the literature [3–7] the ratio of Cr/Fe in the precipitates varies between 0.2–1 for a mean global ratio between 0.5–1. We can assume that the chemical composition of the precipitates depends on the initial ratio of the constituents which is in agreement with the work of Lemaignan and Motta [17] and, of course, of the metallurgical processing.

5. Conclusion

This study shows the efficiency of the concerted application of the SEM and TEM techniques to characterize a microstructure in terms of its crystallographic orientation and chemical composition at two different scales. Individually neither of these techniques can

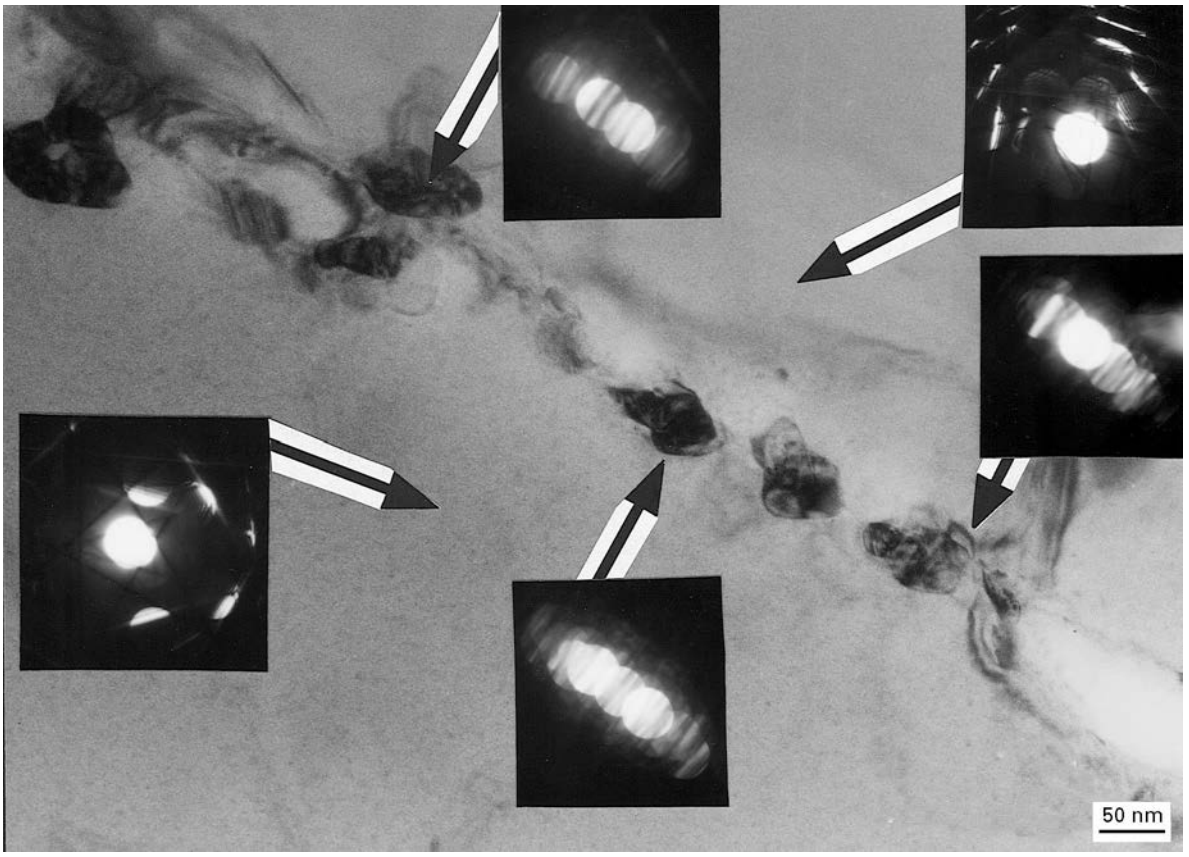

Figure 9 Crystallographic orientation of some precipitates located in the same alignment performed on an area of Fig. 7. The corresponding diffraction pattern area are presented.

TABLE II Chemical composition (at %) of the matrix and precipitates

	Zr	Fe	Cr	Sn
Matrix	99.84	0.01	0.03	0.12
Matrix	99.74	0.06	–	0.24
Precipitate	80.55	13.02	6.47	–
Precipitate	43.19	39.42	17.41	–
Precipitate	53.13	32.46	14.47	–
Precipitate	47.35	35.85	16.82	–

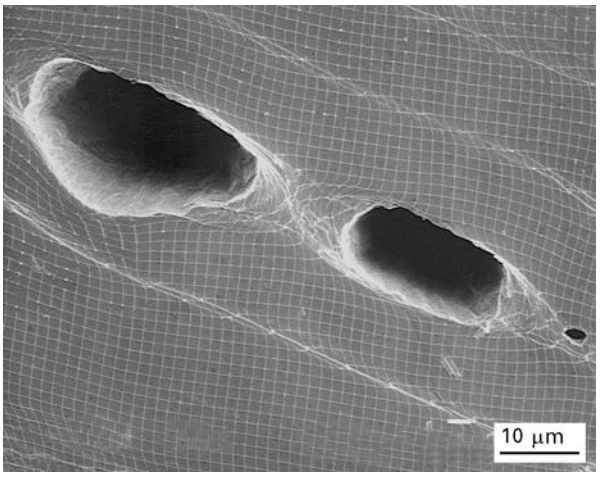

Figure 10 Alignments of damage cavities along the laths boundaries.

give a full picture of a complex microstructure such as that of β treated grade 702 zirconium.

The investigation has revealed the occurrence of a quasi-continuous single crystalline phase, due to the precipitation of the betagenic additional elements (Fe, Cr, Ni) producing the so-called lath boundaries. This phase forms a layer surrounding the laths in the bulk of the material. Its morphology could be assimilated to a net, created by precipitates with a size of several micrometres and linked by narrow bridges with a size of 700 nm. The occurrence of such a phase producing the lath boundaries could explain why damage appears for strains as low as 3% and why it remains located along the lath boundaries (Fig. 10) [18].

Acknowledgements

The authors wish to thank the CEA/CEREM for supplying the studied materials and also financial support. Mr. Pioche (ONERA) is thanked for his assistance with the X-ray microanalysis.

References

1. P. LEMOINE, T. FORGERON, F. LE NAOUR, B. MARINI and M. MOTTOT, in Proceedings of the Journées d'Études sur le Zirconium, École Normale Supérieure de Lyon, October 1990, edited by G. Béranger, P. Lacombe and R. Tricot (Les éditions de physique, Les Ullis, France, 1992) p. 73.
2. J. B. VAN DER SAND and A. L. BEMENT, *J. Nucl. Mater.* **52** (1974) 115.

3. D. ARIAS, T. PALACIOS and C. TURILLO, *ibid* **148** (1987) 227.
4. P. CHEMELLE, D. B. KNORR, J. B. VAN DER SANDE and R. M. PELLOUX, *ibid* **113** (1983) 58.
5. V. KRASEVEC, *ibid* **98** (1981) 235.
6. X. Y. MENG and D. O. NORTHWOOD, *ibid* **132** (1985) 80.
7. R. A. VERSACI and P. IPOHORSKI, *ibid* **80** (1979) 180.
8. W. G. BURGERS, *Physica* **I** (1934) 561.
9. A. AKHTAR, *Metall Trans. A* **7A** (1976) 1735.
10. R. A. HOLT, *J. Nucl. Mater.* **35** (1970) 322.
11. J. P. LANGERON and P. LEHR, *Memoires Scientifiques de la Revue de Metallurgie LVI* **3** (1959) 307.
12. J. CRÉPIN, T. BRETHEAU and D. CALDEMAISON, *Acta Metall. Mater.* **43** (1995) 3709.
13. D. MILLS and G. B. CRAIG, *Trans. AIME* **242** (1968) 1881.
14. P. SOO and G. T. HIGGINS, *Acta Metall.* **16** (1968) 177.
15. R. M. TRECO, in Proceedings of Zirconium and Zirconium Alloys. 8th Western Metal Congress and Exposition, Los Angeles, March 1953 (American Society for Metals, Cleveland, OH, 1953) pp. 254–74.
16. J. FUDENBERGER, M. J. PHILIPPE and C. ESLING, *Scripta Metall.* **24** (1990) pp. 1215–20.
17. C. LEMAIGNAN and A. T. MOTTA, in "Nuclear applications, nuclear materials", **10A**, edited by R. T. Frost, Materials Science and Technology series, edited by R. W. Cahn, P. Haasen and E. J. Kramer (VCH, Weinheim, 1994).
18. J. CRÉPIN, T. BRETHEAU and D. CALDEMAISON, *Acta Metall. Mater.* **44** (1996) 4927.